

Effect of material composition on bending analysis of FG plates via a two-variable refined hyperbolic theory

M. BOUAZZA^{1,2)}, A. M. ZENKOUR^{3,4)}, N. BENSEDDIQ⁵⁾

¹⁾*Department of Civil Engineering
University of Bechar
Bechar 08000, Algeria
e-mail: bouazza_mokhtar@yahoo.fr*

²⁾*Laboratory of Materials and Hydrology (LMH)
University of Sidi Bel Abbes
Sidi Bel Abbes 2200, Algeria*

³⁾*Department of Mathematics
Faculty of Science, King Abdulaziz University
P.O. Box 80203, Jeddah 21589, Saudi Arabia
e-mail: zenkour@kau.edu.sa*

⁴⁾*Department of Mathematics
Faculty of Science
Kafrelsheikh University
Kafrelsheikh 33516, Egypt
e-mail: zenkour@sci.kfs.edu.eg*

⁵⁾*Mechanics Laboratory of Lille
CNRS UMR 8107, University of Lille 1
59655 Villeneuve d'Ascq, France
e-mail: Noureddine.Benseddiq@univ-lille1.fr*

THE MAJOR NOVELTY OF THE ARTICLE IS AN APPLICATION of a two-variable refined hyperbolic shear deformation theory based on studying the bending behavior of functionally graded material (FGM) plates with simply-supported edges. The influence of varying material characteristics and volume fraction of the constituent on bending behavior of the FG plate is examined. The advantage of this theory over other contributions is that a number of functional variables is reduced. All presented problems that have been solved previously, but have not studied the effect on changing plate characteristics, material composition are reinvented.

Key words: FG plate, refined plate theory, bending, plate characteristics.

1. Introduction

ADVANCED MATERIALS HAVE BEEN EXTENSIVELY APPLIED in high performance industrial applications since many years. Among composite materials, functionally graded materials (FGMs) obtained considerable attention for their superior features such as resistance to high temperature environments (better thermal resistance), high wear resistance, among others.

Classical laminated plates suffer from discontinuity of material properties at layer interfaces and constituents of the composite. So, the stresses originate interface issues especially at higher temperature in thermal environments. Such issues can be reduced by the gradually varying volume fraction of the constituent and tailor material for desired applications. At this stage, the graduation of ceramic-metal materials can be varied from one material to the other and so thermal resistance of a constituent is increased due to low thermal conductivity of ceramic. It is interesting to eliminate the low toughness problem of a ceramic material by including a metal material in the constituent.

A vast range of outputs on the linear analysis of FG plates with various theories has been reported by many investigators [1–8]. In such investigations, various plate theories such as classical plate theory (CPT) or higher-order shear deformation plate theory (HPT) are adopted. However, the number of investigators that deal with the nonlinear behaviors of FG plates under transverse mechanical loadings is limited. As an example, Poincare's method is applied by CHI and CHUNG [9, 10] to present the thermally induced large transverse displacement of an FGM thin plate with variable Young's moduli and simply-supported edges. Also, MIZUGUCHI and OHNABE [11] have used a collection of micromechanical and structural processes to discuss the buckling response of FG plates under transverse compressive loadings. BOUAZZA *et al.* [12] have presented the buckling response of FG plates under uniform and linear temperature variations through the thickness with simply-supported edges via the first-order plate theory (FPT). They have discussed stability and compatibility equations according to the von Karman type through their investigation and have observed that transverse shear strains have major effects on critical thermal buckling of the FGM plate. This effect may be obvious for thicker plates or those of larger aspect ratios. BOUAZZA *et al.* [13] have presented the thermal buckling response of simply-supported FG plates via CPT. They supposed inhomogeneous mechanical properties of plates, graded through thickness, according to two types of graduation, namely, power-law and sigmoid FGMs. This plate is considered to have an unchanged temperature rise. A comprehensive study based on the finite element method as well as FPT has been presented by PRAVEEN and REDDY [14] to investigate nonlinear behaviors of FG plates subjected to simultaneous thermal and mechanical loads. PITAKTHAPANAPHONG and BUSSO [15] have investigated the

self-consistent elastoplastic stress solutions for FGM structures under thermal transients.

A three-dimensional (3D) analysis for FG plates, under transverse mechanical loadings has been presented by KASHTALYAN [16]. Also, KASHTALYAN and MENSHEYKOVA [17] have used an extension of this solution to deal with the sandwich panel with a FG core. ZENKOUR [18] has discussed the static behavior of a FG rectangular plate under a transverse mechanical loading with simply-supported edges. He has used a generalized higher-order theory that omits the transverse normal strain. ZENKOUR [19] has compared the benchmark trigonometric and 3-D elasticity solutions for an exponentially graded thick rectangular plate. He [20] also has presented a simplified theory for hygrothermal response of angle-ply composite plates. BATRA and JIN [21] have discussed the FGM plates by changing fiber orientation across the plate thickness. The vibration analysis is discussed based on FEM. The FPT, along with various boundary conditions, has been adopted. QIAN *et al.* [22] have studied static deformations and different types of vibration behavior of a thicker FGM plate using HPT that included a normal effect. They have used the meshless local Petrov–Galerkin method to compute effective material moduli by using Mori–Tanaka homogenization technique [23]. RAMIREZ *et al.* [24] have discussed static behavior of FGM plates. A solution has been derived according to Ritz’s method by applying a discrete layer theory.

The present RPT has only two undetermined variables and it has been proposed by SHIMPI [25] for isotropic plates. After that, it has been extended by SHIMPI and PATEL [26, 27] to deal with the orthotropic plates. The advantages of RPT is that it gives governing equations and constitutive relations in a similar way as in the CPT. It gives results with high accuracy comparing with FPT without including a shear correction factor. Moreover, it compared well with most HPTs and gives accurate and efficient solutions. In this work, the bending response of an FGM plate with simply-supported edges under a transverse sinusoidal load is presented via Navier’s method. Young’s modulus of the FGM plate is supposed to vary continuously across the plate thickness according to various power-law functions. The problem has been solved by using the RPT. The obtained results are validated through a comparison with the corresponding ones in the literature.

2. Analysis of FG plate

2.1. Material graduation

Let us consider an FGM rectangular ($a \times b$) plate with uniform thickness h (see Fig. 1). The proposed FG plate is fabricated of a mixture of metal and ceramic materials. The material composition is varying smoothly along the thickness

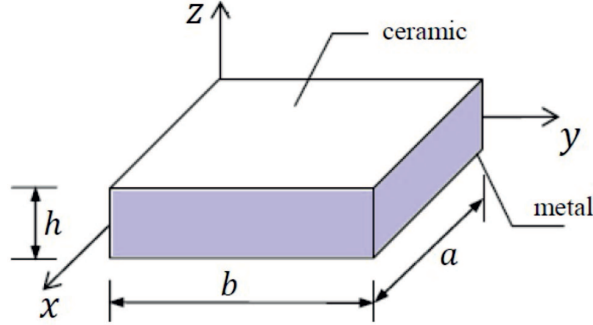


FIG. 1. Typical FGM rectangular plate.

direction only. So, the modulus of elasticity E can be represented by

$$(2.1) \quad E(z) = E_c V_c + E_m V_m, \quad z \in \left[-\frac{h}{2}, \frac{h}{2}\right],$$

where E_c and E_m are Young's moduli of ceramic and metal, V_c and V_m are their volume fractions defined as

$$(2.2) \quad V_c + V_m = 1.$$

The above equations give dimensionless effective Young's modulus in a suitable form

$$(2.3) \quad \bar{E}(z) = \left(\frac{E_c}{E_m} - 1\right) V_c(z) + 1,$$

where $\bar{E}(z) = E(z)/E_m$. Here, we suppose that V_c follows the following various simple-power laws [15, 28]:

$$(2.4) \quad V_c = \begin{cases} \frac{z}{h} + \frac{1}{2}, & \text{linear,} \\ \left(\frac{z}{h} + \frac{1}{2}\right)^2, & \text{quadratic,} \\ 3\left(\frac{z}{h} + \frac{1}{2}\right)^2 - 2\left(\frac{z}{h} + \frac{1}{2}\right)^3, & \text{cubic,} \\ 1 - \left(\frac{1}{2} - \frac{z}{h}\right)^2, & \text{inverse quadratic.} \end{cases}$$

2.2. Basic assumptions

The theory used here is adopted according to the following assumptions:

(i) The displacement components are small comparing with the plate thickness and, therefore, strains involved are infinitesimal.

(ii) The transverse normal stress σ_z is small comparing with in-plane longitudinal and normal stresses σ_x and σ_y and maybe neglected.

(iii) The transverse displacement u_3 may be divided into two components. The first one represents the bending w_b and the other represents the shear w_s . Both w_α , ($\alpha = b, s$) are functions of the coordinates x and y

$$(2.5) \quad u_3(x, y, z) = w_b(x, y) + w_s(x, y).$$

(iv) Both in-plane displacement components u_1 and u_2 are divided into three parts: extension, bending, and shear. That is

$$(2.6) \quad u_1 = u + u_b + u_s, \quad u_2 = v + v_b + v_s.$$

The bending parts u_b and v_b are supposed to be similar, respectively, to the corresponding parts given in CPT. So, the two expressions are written as

$$(2.7a) \quad u_b = -z \frac{\partial w_b}{\partial x}, \quad v_b = -z \frac{\partial w_b}{\partial y}.$$

Also, the shear displacements u_s and v_s give rise, in conjunction with w_s , to the hyperbolic variations of the transverse shear strains γ_{xz} , γ_{yz} and so to the shear stresses τ_{xz} , τ_{yz} through the plate thickness in such a way that τ_{xz} , τ_{yz} are vanished at the lateral faces of the plate. So, these expressions can be represented as

$$(2.7b) \quad u_s = -f(z) \frac{\partial w_s}{\partial x}, \quad v_s = -f(z) \frac{\partial w_s}{\partial y},$$

where

$$(2.7c) \quad f(z) = \frac{2z \sinh\left(\frac{z^2}{h^2}\right)}{2 \sinh\left(\frac{1}{4}\right) + \cosh\left(\frac{1}{4}\right)}.$$

Based on the above assumptions, the displacements of the present RPT can be written according to Eqs. (2.5)–(2.7) as

$$(2.8) \quad \begin{aligned} u_1(x, y, z) &= u(x, y) - z \frac{\partial w_b}{\partial x} - f(z) \frac{\partial w_s}{\partial x}, \\ u_2(x, y, z) &= v(x, y) - z \frac{\partial w_b}{\partial y} - f(z) \frac{\partial w_s}{\partial y}, \\ u_3(x, y, z) &= w_b(x, y) + w_s(x, y). \end{aligned}$$

It is interesting to see that unlike FPT, the present RPT does not involve any shear correction factors. The strain-displacement formulae can be defined

by

$$(2.9) \quad \begin{cases} \varepsilon_x \\ \varepsilon_y \\ \gamma_{xy} \end{cases} = \begin{cases} \varepsilon_x^0 \\ \varepsilon_y^0 \\ \gamma_{xy}^0 \end{cases} + z \begin{cases} \kappa_x^b \\ \kappa_y^b \\ \kappa_{xy}^b \end{cases} + f(z) \begin{cases} \kappa_x^s \\ \kappa_y^s \\ \kappa_{xy}^s \end{cases}, \\ \{\gamma_{xz}, \gamma_{yz}\} = g(z)\{\gamma_{xz}^s, \gamma_{yz}^s\}, \quad \varepsilon_z = 0,$$

where

$$(2.10) \quad \begin{aligned} \varepsilon_x^0 &= \frac{\partial u}{\partial x}, \quad \varepsilon_y^0 = \frac{\partial v}{\partial y}, \quad \gamma_{xy}^0 = \frac{\partial u}{\partial y} + \frac{\partial v}{\partial x}, \\ \kappa_x^\alpha &= -\frac{\partial^2 w_\alpha}{\partial x^2}, \quad \kappa_y^\alpha = -\frac{\partial^2 w_\alpha}{\partial y^2}, \quad \kappa_{xy}^\alpha = -2\frac{\partial^2 w_\alpha}{\partial x \partial y}, \\ \gamma_{xz}^s &= \frac{\partial w_s}{\partial x}, \quad \gamma_{yz}^s = \frac{\partial w_s}{\partial y}, \quad g(z) = 1 - f'(z), \quad \alpha = b, s. \end{aligned}$$

The generalized Hooke's law of an FGM plate gives the following relations

$$(2.11) \quad \begin{cases} \sigma_x \\ \sigma_y \\ \tau_{yz} \\ \tau_{xz} \\ \tau_{xy} \end{cases} = \begin{bmatrix} Q_{11} & Q_{12} & 0 & 0 & 0 \\ Q_{12} & Q_{22} & 0 & 0 & 0 \\ 0 & 0 & Q_{44} & 0 & 0 \\ 0 & 0 & 0 & Q_{55} & 0 \\ 0 & 0 & 0 & 0 & Q_{66} \end{bmatrix} \begin{cases} \varepsilon_x \\ \varepsilon_y \\ \gamma_{yz} \\ \gamma_{xz} \\ \gamma_{xy} \end{cases},$$

where

$$(2.12) \quad Q_{11} = Q_{22} = \frac{E(z)}{1 - \nu^2}, \quad Q_{12} = \nu Q_{11}, \quad Q_{44} = Q_{55} = Q_{66} = \frac{E(z)}{2(1 + \nu)}.$$

2.3. Equilibrium equations

The differential equilibrium equations is derived due to the principle of virtual displacements. It yields

$$(2.13) \quad \iint_{\Omega} \left\{ \int_{-h/2}^{h/2} [\sigma_x \delta \varepsilon_x + \sigma_y \delta \varepsilon_y + \tau_{yz} \delta \gamma_{yz} + \tau_{xz} \delta \gamma_{xz} + \tau_{xy} \delta \gamma_{xy}] dz - q \delta u_3 \right\} d\Omega = 0.$$

The substitution of Eqs. (2.8), (2.9) and (2.11) into Eq. (2.13) and making integration across plate thickness gives

$$(2.14) \quad \begin{aligned} \int_{\Omega} \{ & N_x \delta \varepsilon_x^0 + N_y \delta \varepsilon_y^0 + N_{xy} \delta \gamma_{xy}^0 + M_x^b \delta \kappa_x^b + M_y^b \delta \kappa_y^b \\ & + M_{xy}^b \delta \kappa_{xy}^b + M_x^s \delta \kappa_x^s + M_y^s \delta \kappa_y^s + M_{xy}^s \delta \kappa_{xy}^s + Q_y^s \delta \gamma_{yz}^s \\ & + Q_x^s \delta \gamma_{xz}^s - q(\delta w_b + \delta w_s) \} d\Omega = 0, \end{aligned}$$

in which $(N_x N_y N_{xy})$ represent in-plane force resultants, $(M_x^\alpha, M_y^\alpha, M_{xy}^\alpha)$, $(\alpha = a, b)$ represent the moment resultants and (Q_x^s, Q_y^s) denote the transverse shear stress resultants. All of these resultants are expressed as

$$(2.15) \quad \begin{aligned} \{N_x, N_y, N_{xy}\} &= \int_{-h/2}^{h/2} \{\sigma_x, \sigma_x, \tau_{xy}\} dz, \\ \{M_x^b, M_y^b, M_{xy}^b\} &= \int_{-h/2}^{h/2} \{\sigma_x, \sigma_x, \tau_{xy}\} z dz, \\ \{M_x^s, M_y^s, M_{xy}^s\} &= \int_{-h/2}^{h/2} \{\sigma_x, \sigma_x, \tau_{xy}\} f(z) dz, \\ \{Q_x^s, Q_y^s\} &= \int_{-h/2}^{h/2} \{\tau_{xz}, \tau_{yz}\} g(z) dz. \end{aligned}$$

Also, the substitution of Eq. (2.11) into Eq. (2.15) and making integration across plate thickness gives stress resultants in the form

$$(2.16a) \quad \left\{ \begin{array}{l} \left\{ \begin{array}{l} N_x \\ N_y \\ N_{xy} \end{array} \right\} \\ \left\{ \begin{array}{l} M_x^b \\ M_y^b \\ M_{xy}^b \end{array} \right\} \\ \left\{ \begin{array}{l} M_x^s \\ M_y^s \\ M_{xy}^s \end{array} \right\} \end{array} \right\}$$

$$(2.16b) \quad = \left[\begin{array}{ccc} \left[\begin{array}{ccc} A_{11} & A_{12} & A_{16} \\ A_{12} & A_{22} & A_{26} \\ A_{16} & A_{26} & A_{66} \end{array} \right] & \left[\begin{array}{ccc} B_{11} & B_{12} & B_{16} \\ B_{12} & B_{22} & B_{26} \\ B_{16} & B_{26} & B_{66} \end{array} \right] & \left[\begin{array}{ccc} B_{11}^s & B_{12}^s & B_{16}^s \\ B_{12}^s & B_{22}^s & B_{26}^s \\ B_{16}^s & B_{26}^s & B_{66}^s \end{array} \right] \\ \left[\begin{array}{ccc} B_{11} & B_{12} & B_{16} \\ B_{12} & B_{22} & B_{26} \\ B_{16} & B_{26} & B_{66} \end{array} \right] & \left[\begin{array}{ccc} D_{11} & D_{12} & D_{16} \\ D_{12} & D_{22} & D_{26} \\ D_{16} & D_{26} & D_{66} \end{array} \right] & \left[\begin{array}{ccc} D_{11}^s & D_{12}^s & D_{16}^s \\ D_{12}^s & D_{22}^s & D_{26}^s \\ D_{16}^s & D_{26}^s & D_{66}^s \end{array} \right] \\ \left[\begin{array}{ccc} B_{11}^s & B_{12}^s & B_{16}^s \\ B_{12}^s & B_{22}^s & B_{26}^s \\ B_{16}^s & B_{26}^s & B_{66}^s \end{array} \right] & \left[\begin{array}{ccc} D_{11}^s & D_{12}^s & D_{16}^s \\ D_{12}^s & D_{22}^s & D_{26}^s \\ D_{16}^s & D_{26}^s & D_{66}^s \end{array} \right] & \left[\begin{array}{ccc} H_{11}^s & H_{12}^s & H_{16}^s \\ H_{12}^s & H_{22}^s & H_{26}^s \\ H_{16}^s & H_{26}^s & H_{66}^s \end{array} \right] \end{array} \right] \left\{ \begin{array}{l} \left\{ \begin{array}{l} \varepsilon_x^0 \\ \varepsilon_y^0 \\ \gamma_{xy}^0 \end{array} \right\} \\ \left\{ \begin{array}{l} \kappa_x^b \\ \kappa_y^b \\ \kappa_{xy}^b \end{array} \right\} \\ \left\{ \begin{array}{l} \kappa_x^s \\ \kappa_y^s \\ \kappa_{xy}^s \end{array} \right\} \end{array} \right\}$$

$$(2.16b) \quad \left\{ \begin{array}{l} Q_y^s \\ Q_x^s \end{array} \right\} = \begin{bmatrix} A_{44}^s & 0 \\ 0 & A_{55}^s \end{bmatrix} \left\{ \begin{array}{l} \gamma_{yz}^s \\ \gamma_{xz}^s \end{array} \right\},$$

in which the plate stiffness A_{ij}, B_{ij}, \dots etc. are given by

$$(2.17) \quad \begin{aligned} \{A_{ij}, B_{ij}, D_{ij}, B_{ij}^s, D_{ij}^s, H_{ij}^s\} = \\ \int_{-h/2}^{h/2} Q_{ij} \{1, z, z^2, f(z), zf(z), [f(z)]^2\} dz, \quad i, j = 1, 2, 6, \\ A_{ll}^s = \int_{-h/2}^{h/2} Q_{ll} [g(z)]^2 dz, \quad l = 4, 5. \end{aligned}$$

So, the equilibrium equations may be obtained from Eq. (2.14) after integrating displacement gradients by parts and setting coefficients of δu , δv , δw_b and δw_s to zero individually. So, one obtains

$$(2.18) \quad \begin{aligned} \delta u : \frac{\partial N_x}{\partial x} + \frac{\partial N_{xy}}{\partial y} = 0, \quad \delta v : \frac{\partial N_{xy}}{\partial x} + \frac{\partial N_y}{\partial y} = 0, \\ \delta w_b : \frac{\partial^2 M_x^b}{\partial x^2} + 2 \frac{\partial^2 M_{xy}^b}{\partial x \partial y} + \frac{\partial^2 M_y^b}{\partial y^2} + q = 0, \\ \delta w_s : \frac{\partial^2 M_x^s}{\partial x^2} + 2 \frac{\partial^2 M_{xy}^s}{\partial x \partial y} + \frac{\partial^2 M_y^s}{\partial y^2} + \frac{\partial Q_x^s}{\partial x} + \frac{\partial Q_y^s}{\partial y} + q = 0. \end{aligned}$$

Equations (2.18) may be presented in terms of the variables u , v , w_b and w_s after using different forms of stress resultants from Eq. (2.16). For the present FGM plate, Eqs. (2.18) take the form

$$(2.19a) \quad \begin{aligned} A_{11} \frac{\partial^2 u}{\partial x^2} + A_{66} \frac{\partial^2 u}{\partial y^2} + (A_{12} + A_{66}) \frac{\partial^2 v}{\partial x \partial y} - B_{11} \frac{\partial^3 w_b}{\partial x^3} \\ - (B_{12} + 2B_{66}) \frac{\partial^3 w_b}{\partial x \partial y^2} - B_{11}^s \frac{\partial^3 w_s}{\partial x^3} - (B_{12}^s + 2B_{66}^s) \frac{\partial^3 w_s}{\partial x \partial y^2} = 0, \end{aligned}$$

$$(2.19b) \quad \begin{aligned} A_{66} \frac{\partial^2 v}{\partial x^2} + A_{22} \frac{\partial^2 v}{\partial y^2} + (A_{12} + A_{66}) \frac{\partial^2 u}{\partial x \partial y} - B_{22} \frac{\partial^3 w_b}{\partial y^3} \\ - (B_{12} + 2B_{66}) \frac{\partial^3 w_b}{\partial x^2 \partial y} - B_{22}^s \frac{\partial^3 w_s}{\partial y^3} - (B_{12}^s + 2B_{66}^s) \frac{\partial^3 w_s}{\partial x^2 \partial y} = 0, \end{aligned}$$

$$(2.19c) \quad \begin{aligned} B_{11} \frac{\partial^3 u}{\partial x^3} + (B_{12} + 2B_{66}) \left(\frac{\partial^3 u}{\partial x \partial y^2} + \frac{\partial^3 v}{\partial x^2 \partial y} \right) + B_{22} \frac{\partial^3 v}{\partial y^3} \\ - D_{11} \frac{\partial^4 w_b}{\partial x^4} - 2(D_{12} + 2D_{66}) \frac{\partial^4 w_b}{\partial x^2 \partial y^2} - D_{22} \frac{\partial^4 w_b}{\partial y^4} \\ - D_{11}^s \frac{\partial^4 w_s}{\partial x^4} - 2(D_{12}^s + 2D_{66}^s) \frac{\partial^4 w_s}{\partial x^2 \partial y^2} - D_{22}^s \frac{\partial^4 w_s}{\partial y^4} + q = 0, \end{aligned}$$

$$\begin{aligned}
(2.19d) \quad & B_{11}^s \frac{\partial^3 u}{\partial x^3} + (B_{12}^s + 2B_{66}^s) \left(\frac{\partial^3 u}{\partial x \partial y^2} + \frac{\partial^3 v}{\partial x^2 \partial y} \right) + B_{22}^s \frac{\partial^3 v}{\partial y^3} - D_{11}^s \frac{\partial^4 w_b}{\partial x^4} \\
& - 2(D_{12}^s + 2D_{66}^s) \frac{\partial^4 w_b}{\partial x^2 \partial y^2} - D_{22}^s \frac{\partial^4 w_b}{\partial y^4} + A_{44}^s \frac{\partial^2 w_s}{\partial y^2} + A_{55}^s \frac{\partial^2 w_s}{\partial x^2} \\
& - H_{11}^s \frac{\partial^4 w_s}{\partial x^4} - 2(H_{12}^s + 2H_{66}^s) \frac{\partial^4 w_s}{\partial x^2 \partial y^2} - H_{22}^s \frac{\partial^4 w_s}{\partial y^4} + q = 0.
\end{aligned}$$

2.4. Boundary conditions

For this problem of a simply-supported FG plate we have the following conditions at the plate boundaries:

$$\begin{aligned}
(2.20) \quad & v = w_b = w_s = \frac{\partial w_b}{\partial y} = \frac{\partial w_s}{\partial y} = N_x = M_x^b = M_x^s = 0 \quad \text{at } x = 0, a, \\
& u = w_b = w_s = \frac{\partial w_b}{\partial x} = \frac{\partial w_s}{\partial x} = N_y = M_y^b = M_y^s = 0 \quad \text{at } y = 0, b.
\end{aligned}$$

2.5. Closed-form solution

The present FG rectangular plate has simply-supported edges and its boundary conditions that appeared in Eq. (2.20) can be satisfied by the following expansions:

$$(2.21) \quad \begin{Bmatrix} (w_b, w_s) \\ u \\ v \end{Bmatrix} = \sum_{m=1}^{\infty} \sum_{n=1}^{\infty} \begin{Bmatrix} (W_{bmn}, W_{smn}) \sin(\lambda x) \sin(\mu y) \\ U_{mn} \cos(\lambda x) \sin(\mu y) \\ V_{mn} \sin(\lambda x) \cos(\mu y) \end{Bmatrix},$$

where $\lambda = m\pi/a$ and $\mu = n\pi/b$ and U_{mn} , V_{mn} , W_{bmn} and W_{smn} are arbitrary parameters. The applied transverse load q is also expanded in the double-Fourier series as

$$(2.22) \quad q = \sum_{m=1}^{\infty} \sum_{n=1}^{\infty} Q_{mn} \sin(\lambda x) \sin(\mu y).$$

The substitution of Eqs. (2.21) and (2.22) into Eqs. (2.19) shows that Navier's solution of FG plates can be determined from equations

$$(2.23) \quad \begin{bmatrix} s_{11} & s_{12} & s_{13} & s_{14} \\ s_{12} & s_{22} & s_{23} & s_{24} \\ s_{13} & s_{23} & s_{33} & s_{34} \\ s_{14} & s_{24} & s_{34} & s_{44} \end{bmatrix} \begin{Bmatrix} U_{mn} \\ V_{mn} \\ W_{bmn} \\ W_{smn} \end{Bmatrix} = -Q_{mn} \begin{Bmatrix} 0 \\ 0 \\ 1 \\ 1 \end{Bmatrix},$$

where

$$\begin{aligned}
s_{11} &= A_{11}\lambda^2 + A_{66}\mu^2, & s_{12} &= \lambda\mu(A_{12} + A_{66}), \\
s_{13} &= -\lambda[B_{11}\lambda^2 + (B_{12} + 2B_{66})\mu^2], \\
s_{14} &= -\lambda[B_{11}^s\lambda^2 + (B_{12}^s + 2B_{66}^s)\mu^2], \\
s_{22} &= A_{66}\lambda^2 + A_{22}\mu^2, \\
(2.24) \quad s_{23} &= -\mu[(B_{12} + 2B_{66})\lambda^2 + B_{22}\mu^2], \\
s_{24} &= -\mu[(B_{12}^s + 2B_{66}^s)\lambda^2 + B_{22}^s\mu^2], \\
s_{33} &= D_{11}\lambda^4 + 2(D_{12} + 2D_{66})\lambda^2\mu^2 + D_{22}\mu^4, \\
s_{34} &= D_{11}^s\lambda^4 + 2(D_{12}^s + 2D_{66}^s)\lambda^2\mu^2 + D_{22}^s\mu^4, \\
s_{34} &= H_{11}^s\lambda^4 + 2(H_{12}^s + 2H_{66}^s)\lambda^2\mu^2 + H_{22}^s\mu^4 + A_{55}^s\lambda^2 + A_{44}^s\mu^2.
\end{aligned}$$

3. Numerical results

The proposed mathematical model and solution methodology are used to help a generalized computer program to deal with the bending response of FG plates. Some numerical examples are solved to perform the bending response of the FG plates under transverse sinusoidal load with intensity q_0 at the plate center using the two-variable refined hyperbolic plate theory (RPT).

The dimensionless deflection and stresses are expressed as

$$\begin{aligned}
\bar{w} &= \frac{10h^3 E_c}{a^3 q_0} u_3 \left(\frac{a}{2}, \frac{b}{2} \right), & \bar{w}_b &= \frac{10h^3 E_c}{a^3 q_0} w_b \left(\frac{a}{2}, \frac{b}{2} \right), \\
\bar{w}_s &= \frac{10h^3 E_c}{a^3 q_0} w_s \left(\frac{a}{2}, \frac{b}{2} \right), \\
(3.1) \quad \bar{\sigma}_x &= \frac{h}{aq_0} \sigma_x \left(\frac{a}{2}, \frac{b}{2} \right), & \bar{\sigma}_y &= \frac{h}{aq_0} \sigma_y \left(\frac{a}{2}, \frac{b}{2} \right), \\
\bar{\tau}_{yz} &= \frac{h}{aq_0} \tau_{yz} \left(\frac{a}{2}, 0 \right), & \bar{\tau}_{xz} &= \frac{h}{aq_0} \tau_{xz} \left(0, \frac{b}{2} \right), & \bar{\tau}_{xy} &= \frac{h}{aq_0} \tau_{xy}(0, 0).
\end{aligned}$$

3.1. Validation example

The values obtained for the center deflections using the present two-variable RPT are normalized by dividing the center deflection by that of the classical values. These deflections are reported in Table 1 along with the result of Mindlin's, Reddy's, and Leung's theories [29]. The present results are compared with those of Mindlin's FPT, Reddy's HPT, and Leung's unconstrained HPT for various h/a and b/a ratios. The shear correction factor for Mindlin's FPT is only adopted as $k = 1, 0.82, 0.83$ and 0.84 . Table 1 shows that the present solution gives deflections that agree very well with other solutions.

Table 1. Ratios of mid-span deflections with respect to classical theory ($\nu = 0.2$).

b/a	h/a	Mindlin's theory [29]		Reddy's theory [29]	Leung's theory [29]	Present theory
		$k = 1$	$k = 5/6$			
1	0.05	1.01225	1.01475	1.01468	1.01468	1.0154
	0.10	1.04899	1.05902	1.05860	1.05864	1.0621
	0.15	1.11022	1.13279	1.13142	1.13167	1.1418
	0.20	1.19594	1.23607	1.23273	1.23352	1.2574
	0.25	1.30616	1.36887	1.36203	1.36389	1.4135
4	0.05	1.00682	1.00821	1.00818	1.00818	1.0082
	0.10	1.02727	1.03285	1.03267	1.03268	1.0328
	0.15	1.06135	1.07392	1.07339	1.07344	1.0744
	0.20	1.10907	1.13141	1.13020	1.13037	1.1337
	0.25	1.17042	1.20533	1.20293	1.20337	1.2120

Table 2. Displacement and stresses at particular positions of FG plates under bi-sinusoidal load.

n	Theories	$\bar{w}(0)$	$\bar{\sigma}_y(h/3)$	$\bar{\tau}_{xy}(-h/3)$	$\bar{\tau}_{yz}(h/6)$
1	Generalized TSDT [18]	0.5889	1.4894	0.6110	0.2622
	RMVT-based TSDT [30]	0.5890	1.4898	0.6111	0.2506
	RMVT-based collocation [31]	0.5876	1.5062	0.6112	0.2509
	RMVT-based Galerkin [31]	0.5876	1.5061	0.6112	0.2511
	HSDT [32]	0.5880	1.4888	0.6109	0.2566
	Present	0.5890	1.4899	0.6111	0.2603
2	Generalized TSDT [18]	0.7573	1.3954	0.5441	0.2763
	RMVT-based TSDT [30]	0.7573	1.3960	0.5442	0.2491
	RMVT-based collocation [31]	0.7572	1.4129	0.5437	0.2495
	RMVT-based Galerkin [31]	0.7571	1.4133	0.5436	0.2495
	HSDT [32]	0.7564	1.3940	0.5438	0.2741
	Present	0.7573	1.3962	0.5442	0.2730
4	Generalized TSDT [18]	0.8819	1.1783	0.5667	0.2580
	RMVT-based TSDT [30]	0.8815	1.1794	0.5669	0.2360
	RMVT-based collocation [31]	0.8826	1.1935	0.5674	0.2360
	RMVT-based Galerkin [31]	0.8823	1.1941	0.5671	0.2362
	HSDT [32]	0.8814	1.1755	0.5662	0.2623
	Present	0.8814	1.1796	0.5670	0.2528
8	Generalized TSDT [18]	0.9750	0.9466	0.5856	0.2121
	RMVT-based TSDT [30]	0.9747	0.9477	0.5858	0.2263
	RMVT-based collocation [31]	0.9727	0.9568	0.5886	0.2251
	RMVT-based Galerkin [31]	0.9739	0.9622	0.5883	0.2261
	HSDT [32]	0.9737	0.9431	0.5850	0.2140
	Present	0.9745	0.9479	0.5859	0.2081

Also, Table 2 shows the present refined hyperbolic shear deformation theory results of the displacement and stresses components at the specified positions of

the FG plates with the volume fraction function expressed as $V_c(z) = (z/h + 1/2)^n$ in which $n = 1, 2, 4$ and 8 and $a/h = 10$. The results are compared with the work of aforementioned authors [3–32], and it can be concluded that, in general, the results are in good agreement with all the theories compared in this section, particularly with the results provided by ZENKOUR [18] using the generalized shear deformation theory.

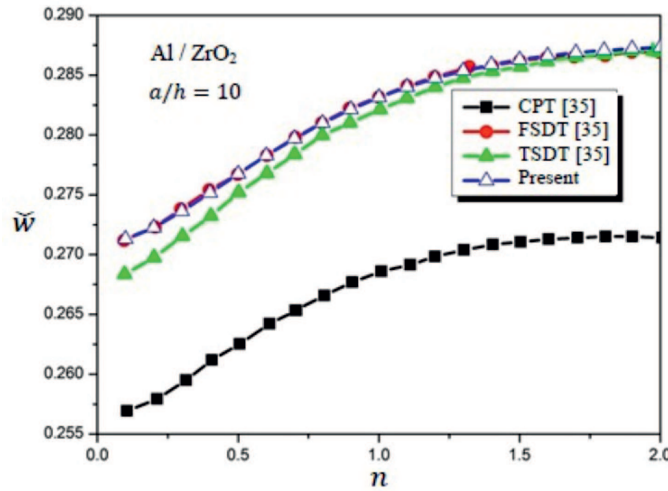


FIG. 2. Variation of non-dimensional central deflection \tilde{w} with power-law index n for a square plate under sinusoidal load.

The non-dimensional central deflection $\tilde{w} = \frac{10^2 E_c h^3}{q a^4} w\left(\frac{a}{2}, \frac{b}{2}, 0\right)$ as a function of the power-law index n and for sidethickness ratio $a/h = 10$ under sinusoidal and distributed loads is given in Fig. 2. The static analysis is conducted using Aluminum (bottom, Al) and Zirconia (top, ZrO_2). The following material properties are used for computing the numerical results: $E_c = 151$ GPa, $E_m = 70$ GPa, $\nu = 0.3$. The obtained results are compared with those predicted by CPT, FSDT and TSDT provided by REDDY [33]. It can be seen that the results of the present theory as well as FST and TSDT are almost identical, and the CPT underestimates the deflection of a plate.

3.2. Bending analysis of FG plates

In this example, the FG rectangular plate is considered to illustrate the proposed method. The combination of materials consists of aluminum and alumina. Young's moduli for both alumina (Al_2O_3) and aluminum (Al) are given, respectively, by $E_c = 380$ GPa and $E_m = 70$ GPa. For both materials, Poisson's ratio is chosen to be fixed as $\nu = 0.3$.

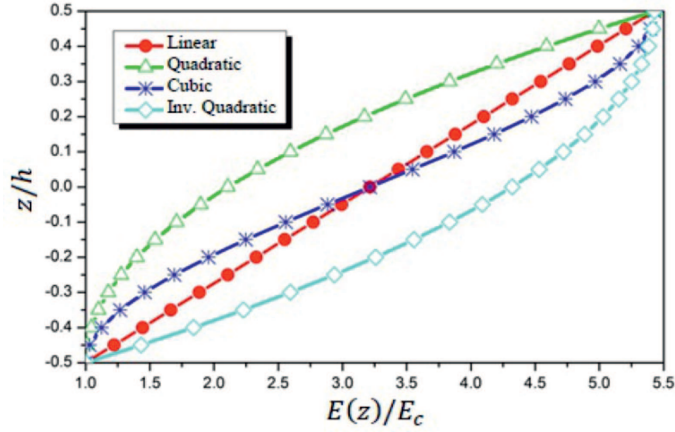


FIG. 3. Variation of the dimensionless Young's modulus ($E(z)/E_c$) in the thickness direction of the FGM plate.

Firstly, variations of dimensionless Young's modulus $\bar{E}(z)$ across the FG plate thickness with linear, quadratic, cubic, and inverse quadratic volume fraction functions are illustrated in Fig. 3. Also, the variations of center deflection \bar{w} of aluminum-alumina FGM plates under sinusoidal loading for various geometric parameters and the volume fraction V_c following simple power laws are illustrated in Figs. 4 and 5. The two cases of isotropic alumina and aluminum correspond to the fully ceramic plate and fully metallic plate, respectively. However, the other cases of FGM plates are summarized as linear, quadratic, cubic, and inverse quadratic. In Figs. 4 and 5, it is obvious that the variation of center deflection \bar{w} of FG plates is greater than that of the fully ceramic plate (Al_2O_3) but smaller than that of the fully metal plate (Al). The variation of the center deflection \bar{w} obtained from the compositional profile is quadratic, greater than linear, cubic and inverse quadratic cases. However, it is clear that the deflections of the inverse quadratic case are smaller than those of the linear and cubic cases, whereas, the deflections of the linear case are smaller than the deflections of the cubic case. Furthermore, a corresponding to the fully ceramic coincides with the compositional profile of FGM plates for the largest value of a/b . In all material cases, the variation of \bar{w} decreases when the geometric parameters a/b and a/h increase.

An analysis of the square homogeneous and the FG plates various functions of the volume fraction, with span-to-thickness ratio $a/h = 10$ on stress distributions through-the-thickness is investigated in Figs. 6–9. As exhibited in Fig. 6, it is found that the longitudinal stress $\bar{\sigma}_x$ corresponding to the quadratic compositional profile gains the maximum compressive value at a ceramic (top) surface

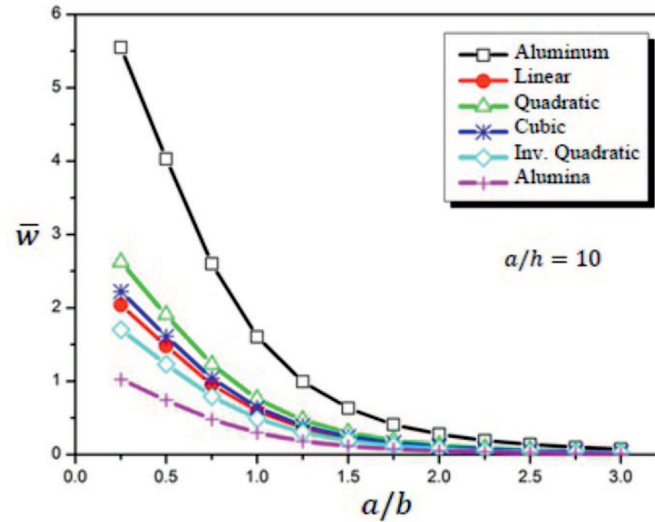


FIG. 4. Non-dimensional center deflection change (\bar{w}) for the metal, ceramic and FGM plates versus the aspect ratio (a/b) with all compositional profiles.

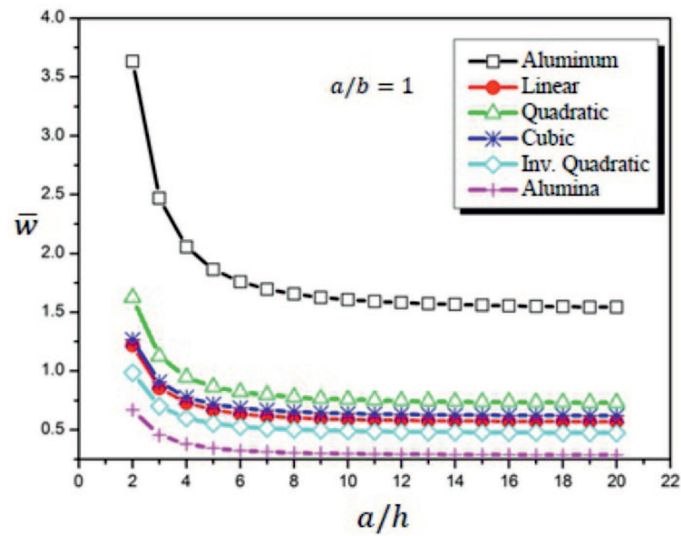


FIG. 5. Non-dimensional the center deflection change (\bar{w}) for the metal, ceramic and FGM plates versus side-to-thickness ratio (a/h) with all compositional profiles.

while the maximum tensile stress is derived for a metallic plate at the bottom surface. However, Fig. 7 shows variation of the in-plane tangential stress $\bar{\tau}_{xy}$ through-the-plate thickness. The stress distribution in aluminum and alumina

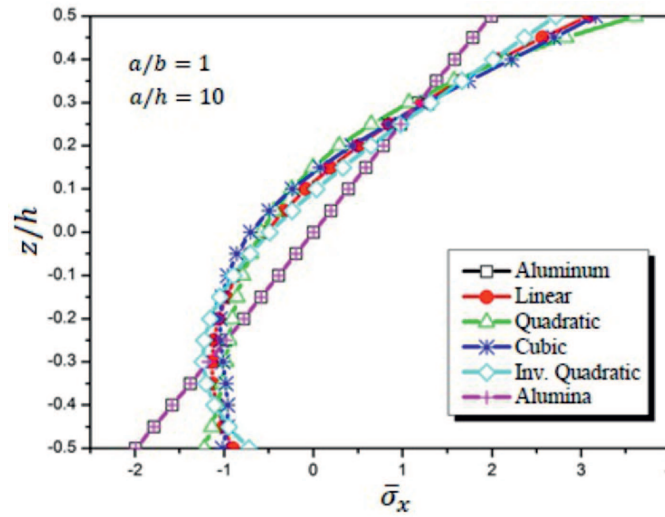


FIG. 6. Variation of in-plane longitudinal stress ($\bar{\sigma}_x$) through the thickness of an FGM plate with all compositional profiles.

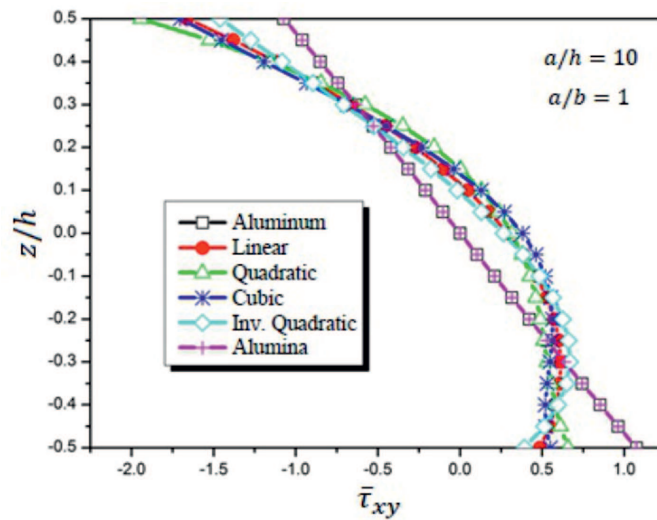


FIG. 7. Variation of transverse shear stress ($\bar{\tau}_{xy}$) through the thickness of an FGM plate with all compositional profiles.

plates is linear; whereas, for FGM, the response is nonlinear and it is governed by variation of properties in the thickness direction. Figure 8 shows variation of the transverse shear stress $\bar{\tau}_{xz}$ across the thickness of the square homogeneous

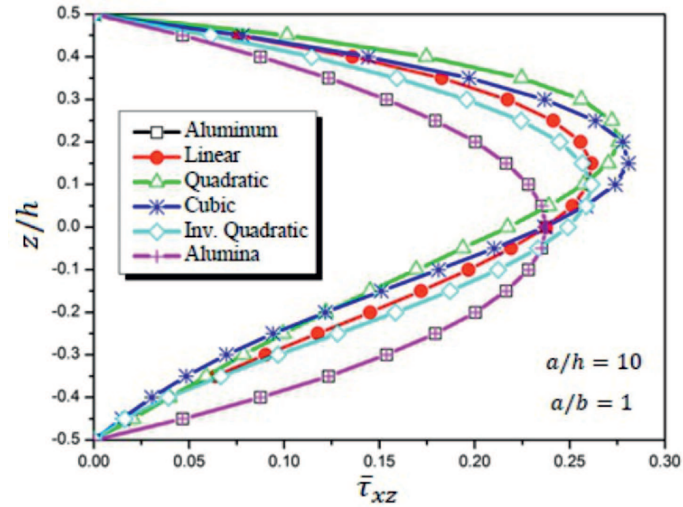


FIG. 8. Variation of transverse shear stress ($\bar{\tau}_{xz}$) through the thickness of an FGM plate with all compositional profiles.

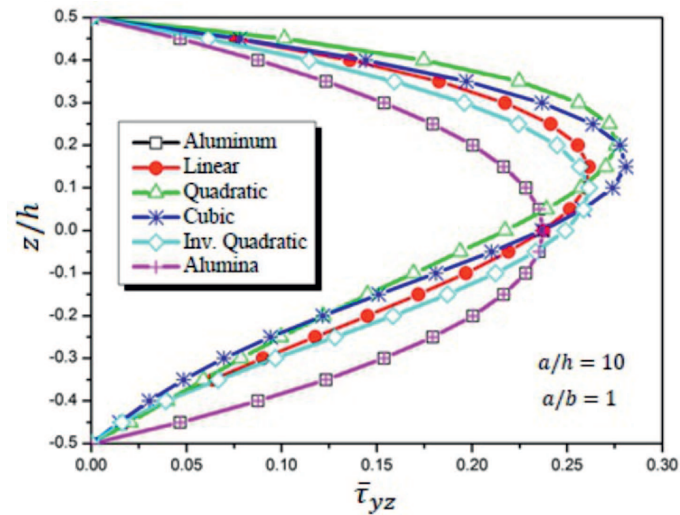


FIG. 9. Variation of transverse shear stress ($\bar{\tau}_{yz}$) through the thickness of an FGM plate with all compositional profiles.

and FG plates, with linear, quadratic, cubic, and inverse quadratic profiles respectively. Figure 9 shows variation of the transverse shear stress $\bar{\tau}_{yz}$ across the thickness of the square homogeneous and FGM plates, with the various volume fraction of constituent materials Fig. 8 and 9 allow themselves to underline their

great influence on transverse shear stresses across the plate thickness. Looking at stresses in Figs. 6–9, we see that the curves for aluminum and alumina coincide. It is also seen that these figures agree well with the results reported in NGUYEN–XUAN *et al.* [34].

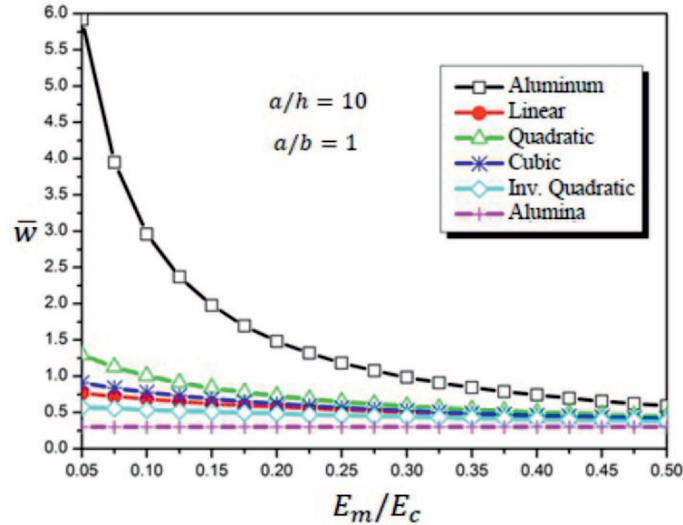


FIG. 10. The effect of material anisotropy on the dimensionless maximum deflection (\bar{w}) of an FGM plate with all compositional profiles

A comparison of center deflections \bar{w} of the FG square plate is made in Fig. 10 for various moduli ratios E_m/E_c ($a/h = 10$). It is clear that with the increasing of the modulus ratio E_m/E_c from 0.05 to 0.5, the deflections \bar{w} decrease steadily. However, it is observed that deflections of the quadratic case are greater than those of cubic, linear, and inverse quadratic cases; whereas, deflections of the inverse quadratic case are lower than those of cubic and linear cases.

Finally, the non-dimensional bending and shear components of vertical displacement versus the aspect ratio a/b and the ratio of moduli E_m/E_c of the plate are plotted in Figs. 11–14. All the displacements decrease with increasing the ratios a/b and E_m/E_c . It is found that the non-dimensional bending \bar{w}_b and shear \bar{w}_s components of vertical displacement of FG plates is higher than that of the fully metal plates but lower than that of the fully ceramic plates. Furthermore, the line corresponding to the cubical compositional profile case coincides with lines for linear compositional profiles for the shear component of the vertical displacement. Comparing Fig. 11 with Fig. 12 and also Fig. 13 with Fig. 14 show that the responses are very similar; however, the bending component of vertical displacement is higher than that of the shear component

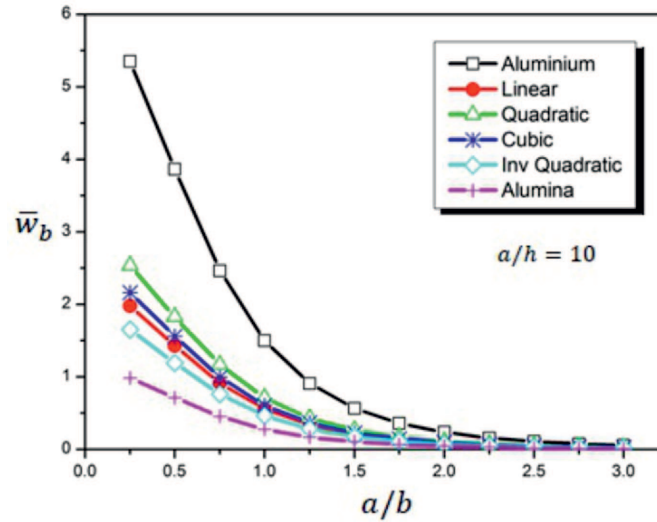


FIG. 11. Non-dimensional bending component (\bar{w}_b) of vertical displacement for the metal, ceramic and FGM plates versus the aspect ratio (a/b) with all compositional profiles.

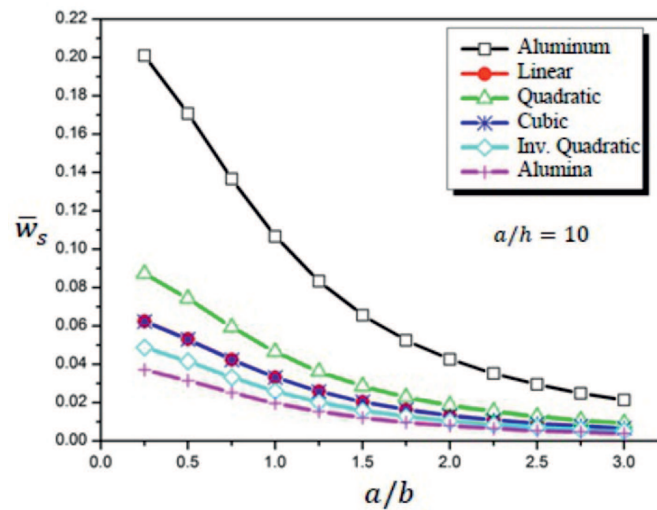


FIG. 12. Non-dimensional shear component (\bar{w}_s) of vertical displacement for the metal, ceramic and FGM plates versus the aspect ratio (a/b) with all compositional profiles.

of vertical displacement. In addition, the in-plane and transverse displacements consist of bending and shear components in which the bending components do not contribute toward shear forces and, likewise, the shear components do not

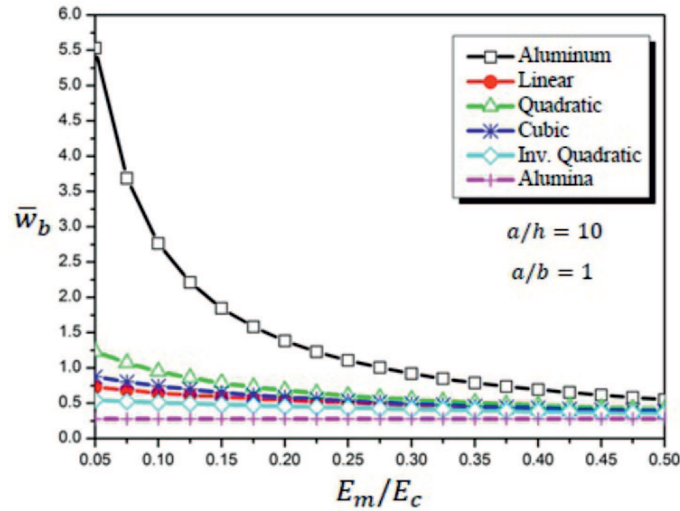


FIG. 13. The effect of material anisotropy on the dimensionless bending component (\bar{w}_b) of vertical displacement of an FGM plate with all compositional profiles.

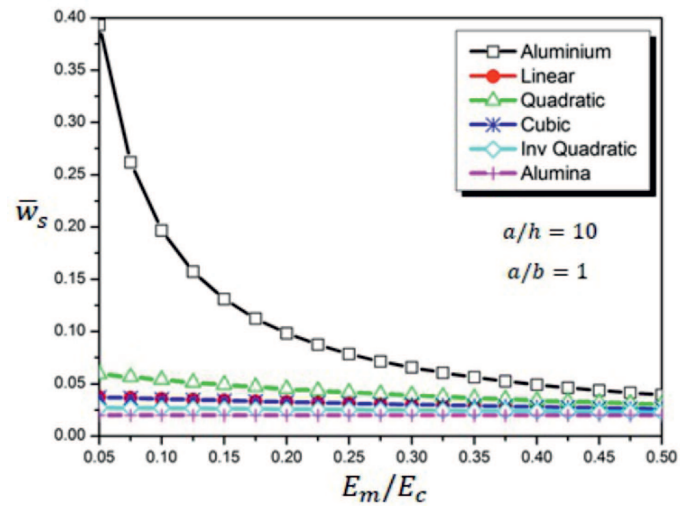


FIG. 14. The effect of material anisotropy on the dimensionless shear component (\bar{w}_s) of vertical displacement of an FGM plate with all compositional profiles.

contribute toward bending moments. By dividing the transverse displacement into the bending shear parts, the number of unknowns of the theory is reduced, thus saving computational time.

4. Conclusions

Bending behaviors of functionally graded material plates have been presented with the help of a two-variable refined hyperbolic theory. Once again, this theory takes under consideration the effect of transverse shears in parabolic distributions across the plate thickness, hence it is needless to use a shear correction factor. The equilibrium equations have strong similarity to those of the classical plate theory. The bending response of FG plates have been analyzed under transverse sinusoidal loading. The gradation of properties across thickness is supposed to be of various power-law functions type (linear, quadratic, cubic, and inverse quadratic) and comparisons are made with homogeneous metal and ceramic isotropic plates. The dimensionless deflection and stresses have been computed for functionally graded plates with ceramic-metal mixture. It is observed that the basic behavior of functionally graded plates that correspond to properties intermediate to that of metal and ceramic, is necessarily laid in between that of ceramic and metal. In conclusion, it can be seen that gradients in material properties play an important role in determining response of functionally graded material plates, and the proposed two-variable refined hyperbolic shear deformation plate theory is accurate and simple in resolving bending responses of functionally graded material plates.

Our objective was so clear from the beginning, examined the influence of the changing plate characteristics material composition and volume fraction of constituent materials on the bending behavior of FGM plates. In addition, utilizing the transverse shear stress hyperbolic function $f(z)$, which gives the bending behavior of functionally graded plates and representation of the transverse shear stress in the thickness of the FGM plate; knowing that different higher order polynomial and trigonometric Sine and exponential functions have already been tried. Moreover, also the use of the hyperbolic function that has already existed, proposed by SOLDATOS [35], and recently, a new theory has been developed by SAYYAD and GHUAL [36] considering a new hyperbolic function but the function in this work is different than the proposed function by SOLDATOS [35], SAYYAD and GHUAL [6].

The results obtained indicate that these proposed refined hyperbolic shear deformation theories are valuable for the investigation of the bending behavior of FGM plates and for this reason in future works. It will be very interesting to assess their capabilities by analyzing new problems (for instance the effect of porosities on the thermo-mechanical bending and the effect of porosities on the thermal buckling behavior of piezoelectric functionally graded plates).

Conflict of interest statement

The authors declare that they have no conflict of interest.

References

1. Z.-H. JIN, G.H. PAULINO, *Transient thermal stress analysis of an edge crack in a functionally graded material*, International Journal of Fracture, **107**, 73–98, 2001.
2. Y.Y. YUNG, D. MUNZ, *Stress analysis in a two materials joint with a functionally graded material. Functional graded materials*, Proceedings of the 4th International Symposium on Functionally Graded Materials, Tsukuba, Japan, 41–46, 1996.
3. Z.-H. JIN, R.C. BATRA, *Stresses intensity relaxation at the tip of an edge crack in a functionally graded material subjected to a thermal shock*, Journal of Thermal Stresses, **19**, 317–339, 1996.
4. Y.-L. CHUNG, S.H. CHI, *The residual stress of functionally graded materials*, Journal of the Chinese Institute of Civil and Hydraulic Engineering, **13**, 1–9, 2001.
5. M. BOUAZZA, A. TOUNSI, E.A. ADDA-BEDIA, A. MEGUENI, *Stability analysis of functionally graded plates subject to thermal loads*, Shell-like Structures-Advanced Structured Materials, **15**, 669–680, 2011.
6. A.M. ZENKOUR, *Bending analysis of functionally graded sandwich plates using a simple four-unknown shear and normal deformations theory*, Journal of Sandwich Structures & Materials, **15**, 6, 629–656, 2013.
7. A.M. ZENKOUR, *A simple four-unknown refined theory for bending analysis of functionally graded plates*, Applied Mathematical Modelling, **37**, 20–21, 9041–9051, 2013.
8. A.M. ZENKOUR, *Bending of FGM plates by a simplified four-unknown shear and normal deformations theory*, International Journal of Applied Mechanics, **5**, 2, 1350020–1350035, 2013.
9. S.H. CHI, Y.-L. CHUNG, *Mechanical behavior of functionally graded material plates under transverse load—Part I: Analysis*, International Journal of Solids and Structures, **43**, 3657–3674, 2006.
10. S.H. CHI, Y.-L. CHUNG, *Mechanical behavior of functionally graded material plates under transverse load – Part II: Numerical results*, International Journal of Solids and Structures, **43**, 3675–3691, 2006.
11. F. MIZUGUCHI, H. OHNABE, *Large deflections of heated functionally graded simply supported rectangular plates with varying rigidity in thickness direction*, Proceedings of the 11th Technical Conference of the American Society for Composites, 957–966, 1996.
12. M. BOUAZZA, A. TOUNSI, E.A. ADDA-BEDIA, A. MEGUENI, *Thermoelastic stability analysis of functionally graded plates: an analytical approach*, Computational Materials Science, **49**, 865–870, 2010.
13. M. BOUAZZA, A. TOUNSI, E.A. ADDA-BEDIA, A. MEGUENI, *Thermal buckling of simply supported FGM square plates*, Applied Mechanics and Materials, **61**, 25–32, 2011.
14. G.N. PRAVEEN, J.N. REDDY, *Nonlinear transient thermoelastic analysis of functionally graded ceramic–metal plates*, International Journal of Solids and Structures, **35**, 4457–4476, 1998.
15. S. PITAKTHAPANAPHONG, E.P. BUSSO, *Self-consistent elasto-plastic stress solutions for functionally graded material systems subjected to thermal transients*, Journal of Mechanics and Physics of Solids, **50**, 695–716, 2002.

16. M. KASHTALYAN, *Three-dimensional elasticity solution for bending of functionally graded rectangular plates*, European Journal of Mechanics - A/Solids, **23**, 853–864, 2004.
17. M. KASHTALYAN, M. MENSHYKOVA, *Three-dimensional elasticity solution for sandwich panels with a functionally graded core*, Composite Structures, **87**, 36–43, 2008.
18. A.M. ZENKOUR, *Generalized shear deformation theory for bending analysis of functionally graded plates*, Applied Mathematical Modelling, **30**, 67–84, 2006.
19. A.M. ZENKOUR, *Benchmark trigonometric and 3-D elasticity solutions for an exponentially graded thick rectangular plate*, Archive of Applied Mechanics, **77**, 197–214, 2007.
20. A.M. ZENKOUR, *Simplified theory for hygrothermal response of angle-ply composite plates*, AIAA Journal, **52**, 1466–1473, 2014.
21. R.C. BATRA, J. JIN, *Natural frequencies of a functionally graded anisotropic rectangular plate*, Journal of Sound and Vibration, **282**, 509–516, 2005.
22. L.F. QIAN, R.C. BATRA, L.M. CHEN, *Static and dynamic deformations of thick functionally graded elastic plates by using higher-order shear and normal deformable plate theory and meshless local Petrov–Galerkin method*, Composites B, **35**, 685–697, 2004.
23. T. MORI, K. TANAKA, *Average stress in matrix and average elastic energy of materials with misfitting inclusions*, Acta Metallurgica, **21**, 571–574, 1973.
24. F. RAMIREZ, P.R. HEYLIGER, E. PAN, *Static analysis of functionally graded elastic anisotropic plates using a discrete layer approach*, Composites B, **37**, 10–20, 2006.
25. R.P. SHIMPI, *Refined plate theory and its variants*, AIAA Journal, **40**, 137–146, 2002.
26. R.P. SHIMPI, H.G. PATEL, *A two variable refined plate theory for orthotropic plate analysis*, International Journal of Solids and Structures, **43**, 6783–6799, 2006.
27. R.P. SHIMPI, H.G. PATEL, *Free vibrations of plate using two variable refined plate theory*, Journal of Sound Vibration, **296**, 979–999, 2006.
28. A.H. SOFIYEV, A. DENIZ, I.H. AKÇAY, E. YUSUFOĞÇLU, *The vibration and stability of a three-layered conical shell containing an FGM layer subjected to axial compressive load*, Acta Mechanica, **183**, 129–144, 2006.
29. A.Y.T. LEUNG, *An unconstrained third-order plate theory*, Computers and Structures, **40**, 871–875, 1991.
30. C.P. WU, H.Y. LI, *An RMVT-based third-order shear deformation theory of multilayered functionally graded material plates*, Composite Structures, **92**, 2591–605, 2010.
31. C.P. WU, K.H. CHIU, Y.M. WANG, *RMVT-based meshless collocation and element-free Galerkin methods for the quasi-3D analysis of multilayered composite and FGM plates*, Composite Structures, **93**, 923–943, 2011.
32. J.L. MANTARI, A.S. OKTEM, C. GUEDES SOARES, *Bending response of functionally graded plates by using a new higher order shear deformation theory*, Composite Structures, **94**, 714–723, 2012.
33. J.N. REDDY, *Analysis of functionally graded plates*, International Journal for Numerical Methods in Engineering, **47**, 663–684, 2000.
34. H. NGUYEN-XUAN, L.V. TRAN, T. NGUYEN-THOI, H.C. VU-DO, *Analysis of functionally graded plates using an edge-based smoothed finite element method*, Composite Structures, **93**, 3019–3039, 2011.

-
35. K.P. SOLDATOS, *A general laminated plate theory accounting for continuity of displacements and transverse shear stresses at material interfaces*, Composite Structures, **20**, 195–211, 1992.
 36. A.S. SAYYAD, Y.M. GHUAL, *Flexure of thick beams using new hyperbolic shear deformation theory*, International Journal of Mechanics, **5**, 3, 113–122, 2011.

Received August 6, 2017; revised version March 8, 2018.
